Supporting Information

Inner-Structure and Outer-Pressure Synergistically Trigger Highly Efficient Luminescence in Antimony Based Perovskites

Xiaoming Zhang [a], Bihao Zhuang [a], Qinglin Meng [a], Ziqiao Wu [b], Zhiyan Yi [a], Panheng Wang [a], Jiayi Li [a], Jiandong Fan*[, a, b,c], Wenzhe Li*[, a, b,c]

[a] Institute of New Energy Technology, Jinan University, Guangzhou 510632, China

[b] Institute of New Energy Technology, College of Physics & Optoelectronic Engineering, Jinan University, Guangzhou, 510632, China.

[c] Guangdong Provincial Key Laboratory of Nanophotonic Manipulation, Jinan University, Guangzhou 511443, China.

E-mail: (Jiandong Fan) jdfan@jnu.edu.cn; (Wenzhe Li) li_wz16@jnu.edu.cn.

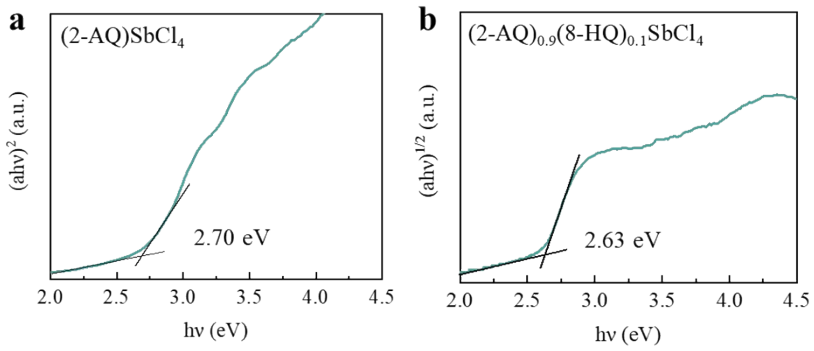

Fig. S1. Absorption spectra of (a) $(2\text{-AQ})SbCl_4$ and (b) $(2\text{-AQ})_{0.9}(8\text{-HQ})_{0.1}SbCl_4$ single crystal.

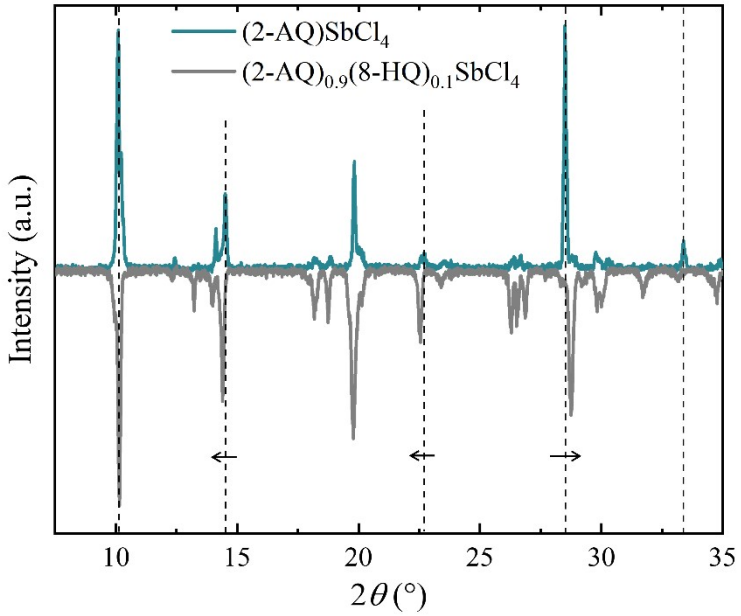

Fig. S2. The XRD patterns of (a) $(2\text{-AQ})SbCl_4$ and (b) $(2\text{-AQ})_{0.9}(8\text{-HQ})_{0.1}SbCl_4$ single crystal. The diffraction peaks of 14.12°, 22.53° move to the low-angle region, in the counterpart, the peak of 28.56° shifts to the large angle region.

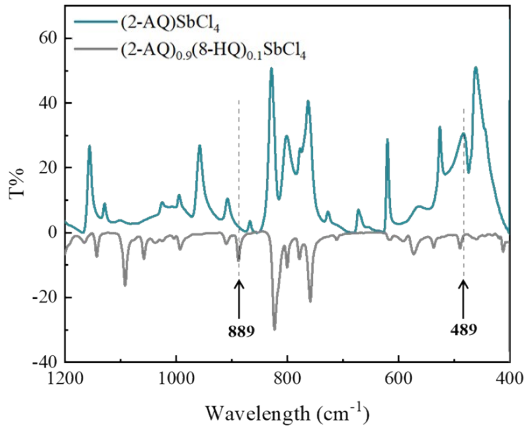

Fig. S3. FTIR spectra of (a) (2-AQ)$SbCl_4$ and (b) $(2\text{-AQ})_{0.9}(8\text{-HQ})_{0.1}SbCl_4$ single crystal. As labeled in the FTIR spectra, the $\delta_{(OH)}$ out of plan and $\delta_{(C\text{-}O)}$ in 8-HQ can be clearly identified at the wave number of 889 and 489 cm^{-1}, respectively. [1]

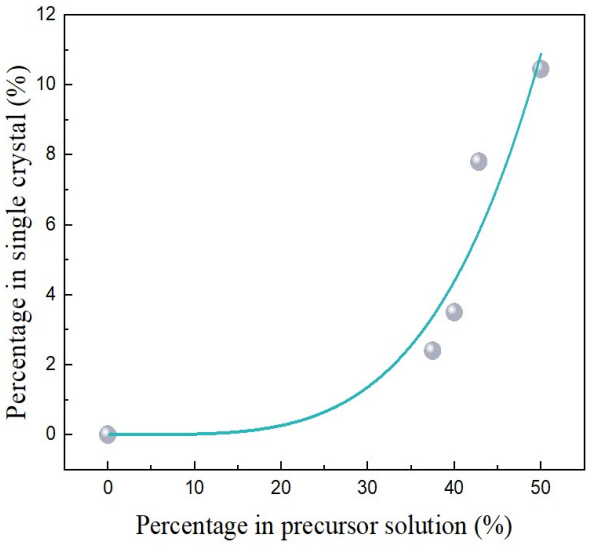

Fig. S4. The points in diagram reflects the relationship between feeding and actual measured content of 8-HQ. The content of 8-HQ is calculated from O and N element ratio, which is obtained from organic element analyzer. We fitted the curve following the formula: $y=1.302\times10^{-6}\times x^{4.074}$.

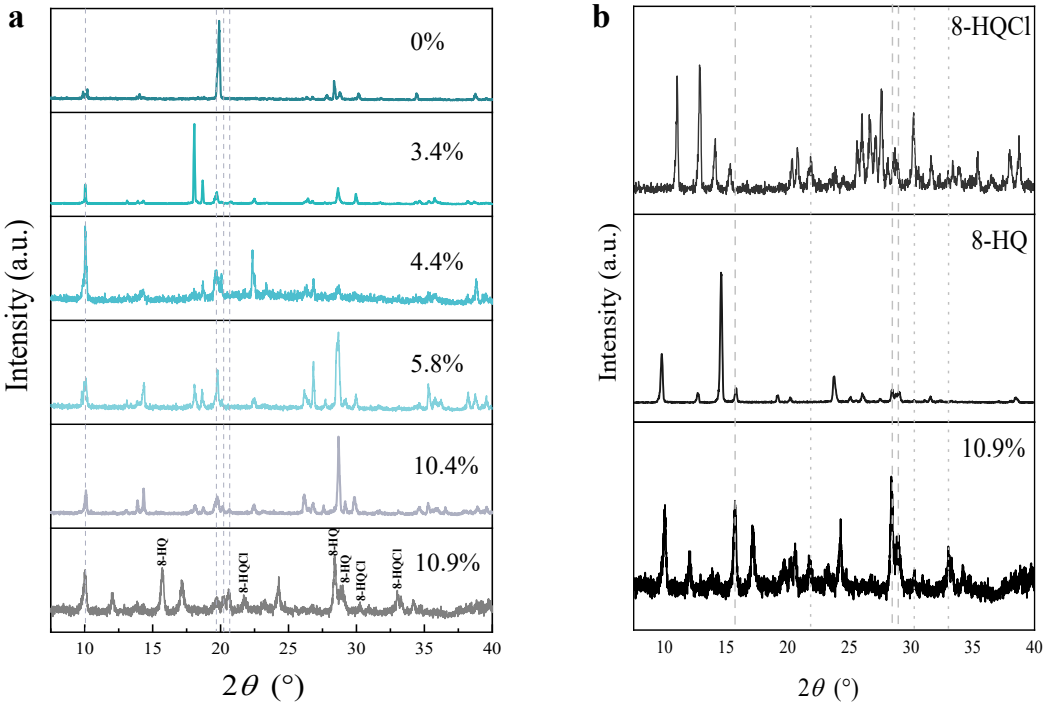

Fig. S5. (a) XRD patterns of $(2\text{-AQ})_{1-x}(8\text{-HQ})_xSbCl_4$ single crystal with various 8-HQ contents. (b) XRD patterns of $(2\text{-AQ})_{0.891}(8\text{-HQ})_{0.109}SbCl_4$, 8-HQ and 8-HQ hydrochloride salt. When the 8-HQ content higher than 10.4%, we can see numerous impurity peaks. Through the comparation with 8-HQ and 8-HQCl, it is observed that the impurity peaks meanly come from the above two compounds. This result gives good explanation for why the luminous efficiency decreases at high doping concentrations.

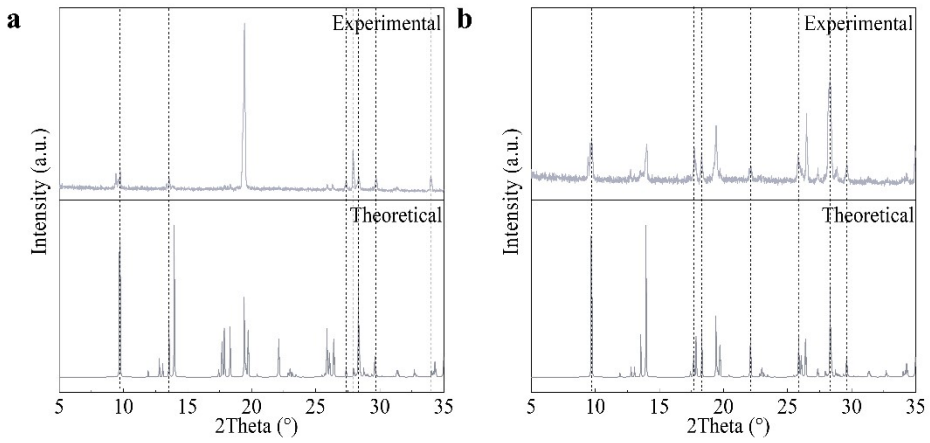

Fig. S6. XRD patterns of (a) (2-AQ)$SbCl_4$ and (b) $(2\text{-AQ})_{0.9}(8\text{-HQ})_{0.1}SbCl_4$ single crystal. The experimental patterns are the XRD results characterized by fine crystal and the theoretical patterns are calculated from single crystal data.

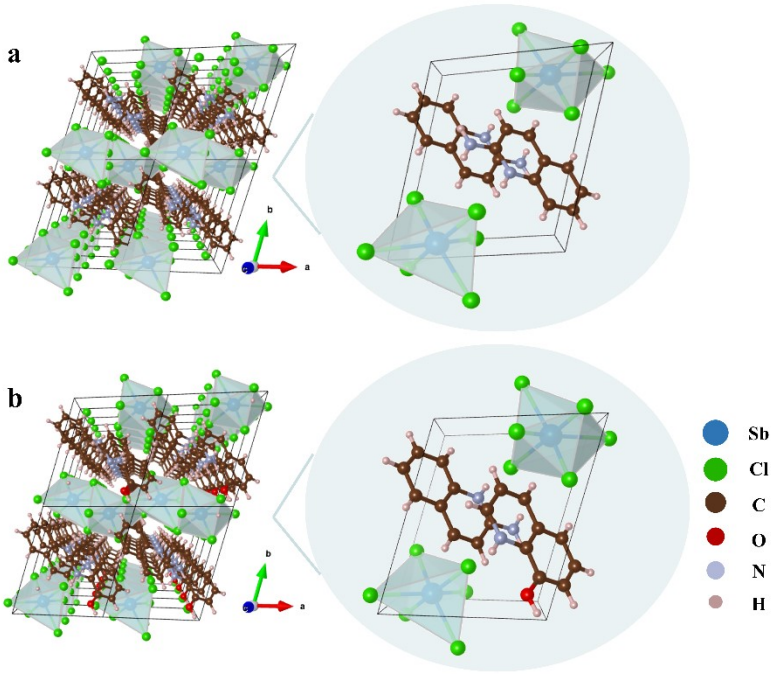

Fig. S7. Schematic diagram of (a) (2-AQ)$SbCl_4$ and (b) $(2\text{-AQ})_{0.9}(8\text{-HQ})_{0.1}SbCl_4$ single crystals along the [00h] crystallographic orientation.

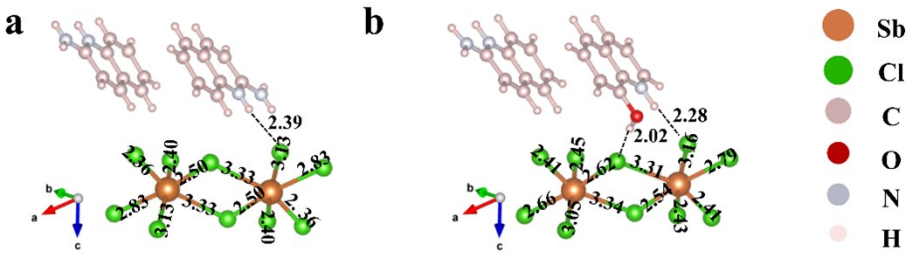

Fig. S8. The schematic diagram of the H-bond between Sb-Cl octahedron and organic compounds in (a) (2-AQ)$SbCl_4$ and (b) $(2\text{-AQ})_{0.9}(8\text{-HQ})_{0.1}SbCl_4$ single crystal.

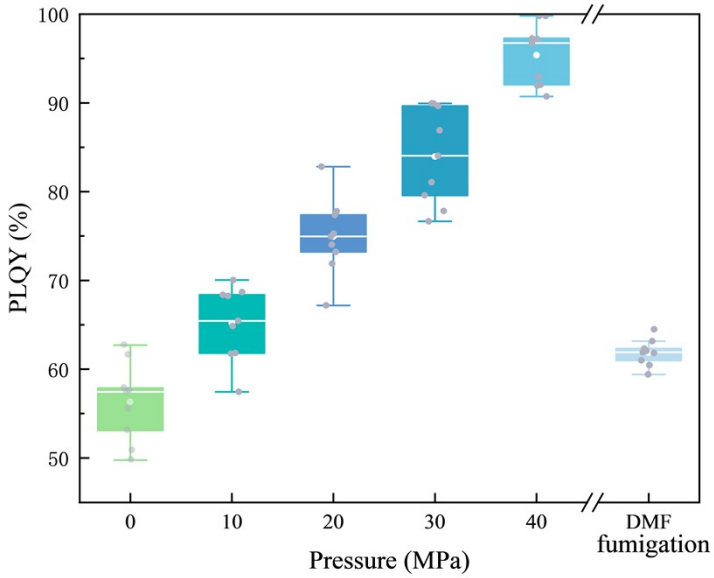

Fig. S9. PLQY values of $(2\text{-AQ})_{0.9}(8\text{-HQ})_{0.1}SbCl_4$ materials under different degree of pressure and after DMF solvent fumigation.

Fig. S10. The digital images of the $(2\text{-AQ})_{0.9}(8\text{-HQ})_{0.1}SbCl_4$ powders merged in DMF, DMSO and MeCN atmospheres.

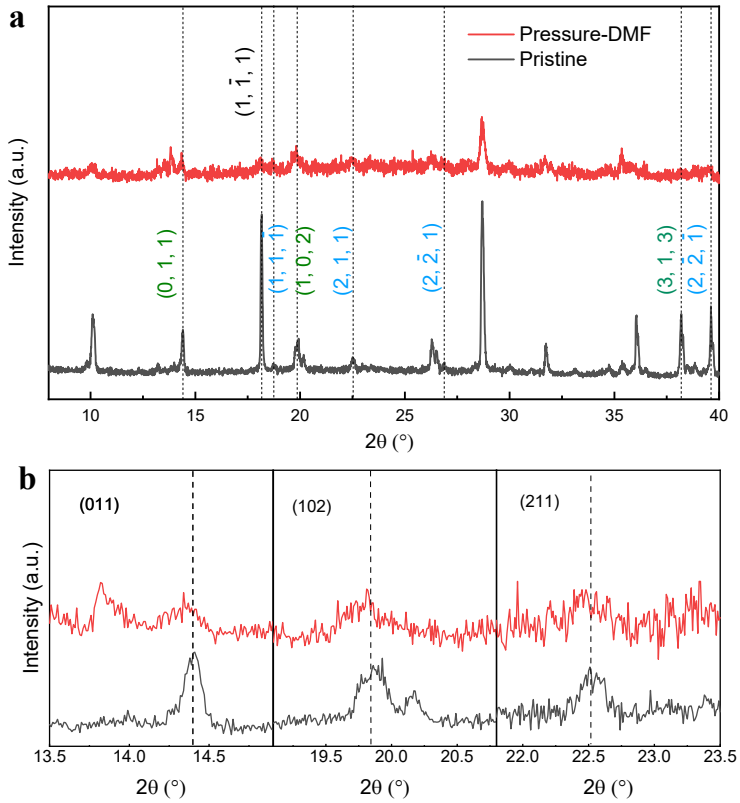

Fig. S11. (a) The powder XRD patterns of $(2\text{-AQ})_{0.9}(8\text{-HQ})_{0.1}SbCl_4$ powder with pressure application and furtherly treated with DMF vapor. (b) the (011), (102) and (102) crystal facets patterns.

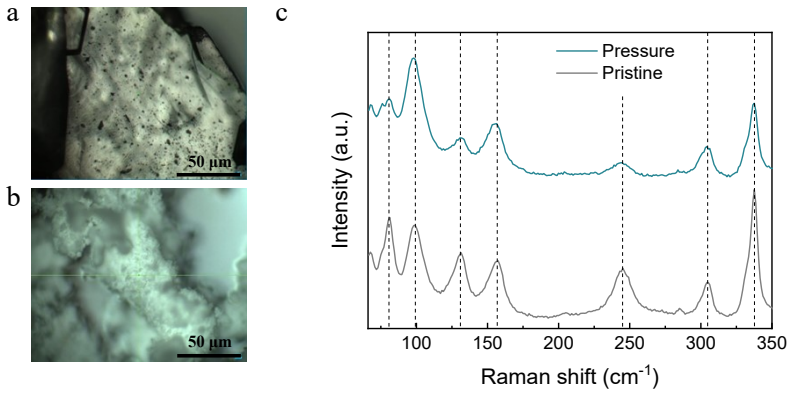

Fig. S12. (a) Microscopic image of $(2\text{-AQ})_{0.9}(8\text{-HQ})_{0.1}SbCl_4$ single crystal without pressure application, (b) Microscopic image of $(2\text{-AQ})_{0.9}(8\text{-HQ})_{0.1}SbCl_4$ powders with pressure application, (c) the corresponding RAMAN spectra of the $(2\text{-AQ})_{0.9}(8\text{-HQ})_{0.1}SbCl_4$ with and without pressure application.

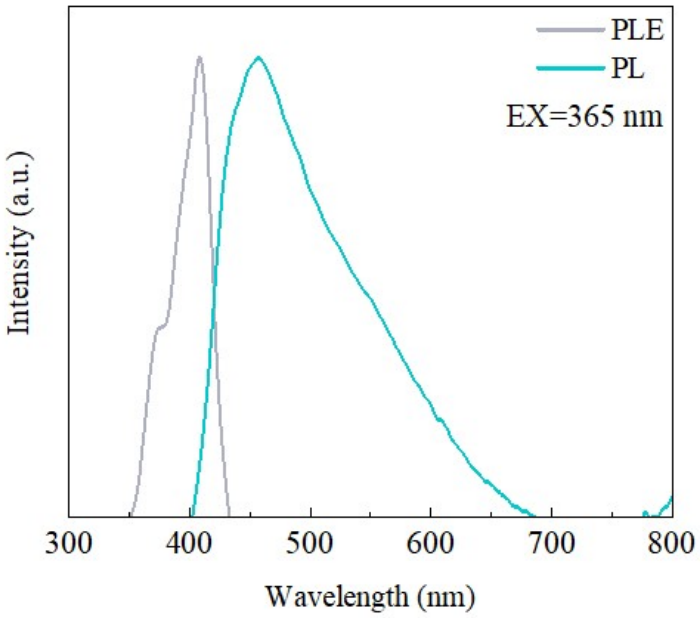

Fig. S13. PL and PLE spectra of the (2-AQ)Cl powders.

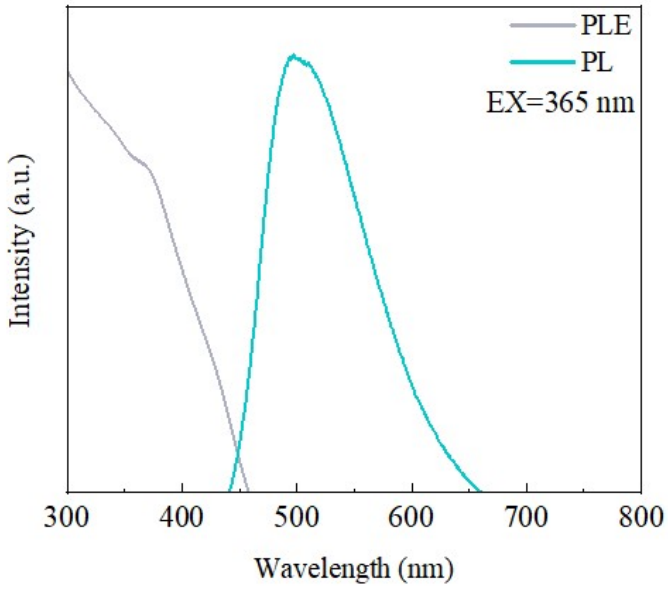

Fig. S14. PL and PLE spectra of the (8-HQ)Cl·H_2O powders.

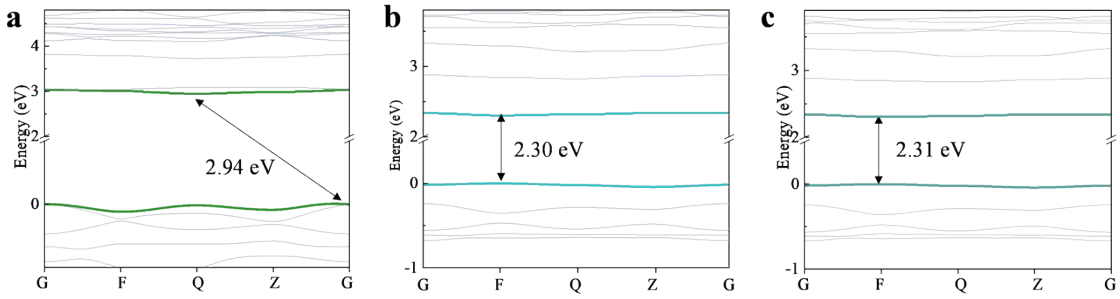

Fig. S15. Band structure calculated by the GGA-PBE exchange-correlation functional of (a) (2-AQ)$SbCl_4$, (b) $(2\text{-AQ})_{0.9}(8\text{-HQ})_{0.1}SbCl_4$ and (c) $(2\text{-AQ})_{0.9}(8\text{-HQ})_{0.1}SbCl_4$ with pressure application.

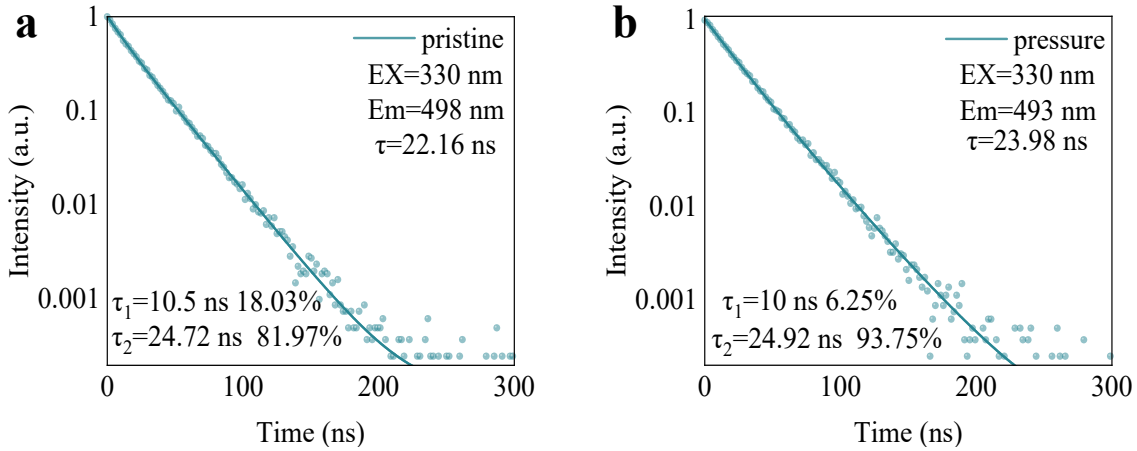

Fig. S16. TRPL spectra of (a) $(2\text{-AQ})_{0.9}(8\text{-HQ})_{0.1}SbCl_4$ and (b) $(2\text{-AQ})_{0.9}(8\text{-HQ})_{0.1}SbCl_4$ with pressure application. The points are fitted by quadratic exponential decay function.

Table S1. Details of X-ray crystallographic parameters of (2-AQ)$SbCl_4$ and $(2\text{-AQ})_{0.9}(8\text{-HQ})_{0.1}SbCl_4$ perovskite single crystals.

Formula	(2-AQ)$SbCl_4$	$(2\text{-AQ})_{0.9}(8\text{-HQ})_{0.1}SbCl_4$
CCDC No.	2407443	2407444
Measurement temperature (K)	293(2)	
Crystal system	triclinic	
Space group name	$P\bar{1}$	
Lattice parameters	a = 8.1635(4) Å b = 9.5360(4) Å c = 9.5703(4) Å α = 86.176(4)° β = 71.264(4)° γ = 73.032(4)°	a = 8.18950(10) Å b = 9.50370(10) Å c = 9.6114(2) Å α = 86.3010(10)° β = 70.882(2)° γ = 73.3260(10)°
Unit-cell volume	674.53(6) $Å^3$	676.72(2) $Å^3$
Z	2	2
Final R indexes [All data]	R1= 0.0375 wR^2 = 1.053	R1= 0.0327 wR^2 = 1.039
Goodness-of-fit on F^2	1.053	1.037

Table S2. Summary of the luminous characteristics of high-performance Sb-based perovskites (PLQY≥85%) reported before

compound	PLQY / %	Wavelength / nm
$(PPN)_2SbCl_5$	98.1	635
$(Bzmim)_2SbCl_5$	86.3	583
$(TPA)_2SbCl_5$	95.3	610
$(CTP)_2SbCl_5$	96.8	620
$(Me_3BzN)SbCl_5$	95.3	620
$(Et_3BzN)SbCl_5$	97	589
$(Pr_3BzN)SbCl_5$	96.3	640
$(Et_4N)SbCl_5$	97.3	627
$(Pr_4N)SbCl_5$	94.9	610
$(C_9NH_{20})_2SbCl_5$	98	590
$(Ph_4P)_2SbCl_5$	87	650
$(DTA)_2SbCl_5 \cdot DTAC$	90	620
$(HL)_3SbCl_5 \cdot Cl$	99	566
$(2\text{-AQ})_{0.9}(8\text{-HQ})_{0.1}SbCl_4$ (This work)	99.8	495

References:

1. R. B. Debabis, W. Amamou, N. Chniba-Boudjada and F. Zouari, *J Phys Chem Solids*, 2019, **124**, 296-304.